Soft Matter

Accepted Manuscript

ROYAL SOCIETY OF CHEMISTRY

www.rsc.org/softmatter

The Effect of Position of (*S*)-2-Octyloxy Tail on the Formation of Frustrated Blue Phase and Antiferroelectric Phase in Schiff Base Liquid Crystals

Chiung-Cheng Huang*, Ching-Chung Hsu, Li-Wen Chen, Yu-Lun Cheng

Department of Chemical Engineering, Tatung University, Taipei 104, Taiwan, R.O.C.

Keywords: Intramolecular hydrogen bonding, Schiff base, Salicylaldimine, Blue phase and Antiferroeletric phase

Abstract

Two series of chiral salicylaldimine-based liquid crystals which differ from each other in the position of (*S*)-2-octyloxy tail have been synthesized and characterized by polarizing optical microscopy, differential scanning calorimetry, electrical switching. Compounds **OH I(n=6-7)** having (*S*)-2-octyloxy tail close to the salicylaldimine core and compounds **OH II(n=6-11)** having (*S*)-2-octyloxy tail far from the salicylaldimine core exhibit polymorphism of mesophases including frustrated blue phase and antiferroelectric (SmC_A^*) phases. Notably, as compared with structurally similar Schiff base compounds **H I (n=7)**, intramolecular hydrogen

bonding in antiferroelectric salicylaldimine-based compounds **OH I (n=7)** induces frustrated blue phase. However, as compared with structurally similar Schiff base compounds **OH II (n=8)**, the lack of intramolecular hydrogen bonding in Schiff base compounds **H II (n=8)** suppresses antiferroelectric properties.

I Introduction

Chirality and liquid crystals are both widely manifested in nature and biology. Chiral liquid crystal materials have been attracting significant attention because of the discoveries of the ferroelectric (SmC^*), antiferroelectric (SmC_A^*), ferrielectric (SmC_r^*), twist grain boundary phase (TGB^*) and blue phases (BPs), and the potential for the application in the electro-optical devise.[1] Both blue phases and twist grain boundary phases are two kinds of frustrated structures that can be induced by chiral groups in liquid crystals. Blue phases are usually found between the isotropic liquid and cholesteric phase of short pitches. According to the characteristic of double twist helical structure, they are classified as blue phase III(BPIII), blue phase II(BPII) and blue phase I(BPI), which appear as the temperature decreases from isotropic liquid phase.[2,3] The packing structures are macroscopically amorphous, simple cubic, body-centered cubic, respectively. Blue phases are potentially useful for fast light modulators or tunable photonic crystals in applications. However, they are usually observed in very narrow temperature range in a single molecule, which

limit their practical applicability.[4] Therefore, both stabilization and broadening of the temperature range of blue phase are the most important issues and attracting significant attention.[3,5-20] There are several different methods to broaden blue phase range.[5-18] The most popular way to induce blue phase is the addition of a sufficient amount of chiral dopant into achiral LC hosts. For synthetic chemists, it can be achieved by incorporating optically pure groups into the geometric structures of liquid crystal molecule.[14,19-25] Consequently, chirality plays an important role in BPs.[26,27]

The best known smectic phases are the ferroelectric chiral smectic C (SmC^*) phase and antiferroelectric chiral smectic C (SmC_A^*) phase. In the SmC^* phase the chiral molecules tilt with respective to the layers normal. In contrast, the tilting direction of the chiral molecules in the SmC_A^* phase alternates in a zig-zag mode between the layers. Antiferroelectric (SmC_A^*) phase in the chiral liquid crystals exhibiting a DC threshold, double hysteresis, and tristable switching properties[28-30] has been demonstrated to have the potential in the field technology. And the correlation between the molecular structure of the materials and the appearance of the antiferroelectric liquid crystals has been primarily successfully established.[31-33] It has been generally concluded that a rod-like molecule is make up of a three-ring core, with at least two rings that are not directly linked, and a chiral tail with a

transversal disposition concerning the long molecular axis and connected to rigid core through a carboxylate linkage. The dipole-associated functional groups such as ester or amido groups are the main types of connectors within the cores. And the formation of the SmC_A^* phase in chiral liquid crystals also depends strongly on the high chirality of the molecules.

The possibility of getting both frustrated BP and antiferroeletric SmC_A^* phase in a rod-like molecule turned out to be difficult. It is probably due to both of frustrated BP and nematic phase possessing long-range order of the mean orientations, but lacking any long-range translational order. In contrast, antiferroeletric SmC_A^* phase demands an exceptionally long-range of translational order along the smectic layer normal. Consequently only a few single chiral rod-like materials possessing both frustrated BP and SmC_A^* phases have been reported. In 1998, Li *et al*. synthesized a cyclohexane-based trimesogen is the first oligomeric antiferroelectric liquid crystal that exhibits a fairly rich polymorphism of mesophases including frustrated blue phase.[34] Lagerwall *et al.* have presented a chiral twin dimer with the change of the molecular conformation from the rod to bent shape on cooling possessed smectic blue phase and antiferroeletric property.[35] Moreover, Wu have reported two antiferroelectric rod-like molecules with two asymmetric carbons represent another two frustrated phase, BP and $TGBA^*$

phases.[36,37]

Schiff base (azomethine) has been widely employed as a linking group in the synthesis of many forms of liquid crystals.[1] Its analogues, salicylaldimine[*N*-(2-hydroxy-4-alkoxybenzylidene) aniline] compounds are more stable to heat and moisture due to the presence of intramolecular hydrogen bonding between the hydroxy group and the imine group. In addition, with their synthetic versatility and ability to coordinate metals, they have been also employed in the synthesis of metallomesogens.[38] Generally speaking, rod-liked Schiff base liquid crystals exhibited nematic and/or smectic mesophases.[1,38] With introducing asymmetric carbons centers in the form of chiral alkyl tail or present within the molecule, frustrated mesophases and new phase sequences have been discovered in Schiff base compounds. Such as a monosubstituted ferrocene-based Schiff base derivative tethering (*S*)-2-methylbutoxy tail, the first chiral metallomesogen[39] exhibited two frustrated phases, BP and TGBA* phases. Moreover, Schiff base pro-mesogenic unit could also be an electron rich moiety that links cholesteryl ester unit through a flexible polymethylene spacer to obtain unsymmetrical dimesogen compounds possessing frustrated BP and TGBA* phases[5]. On the other hand, a few chiral Schiff base liquid crystals consist of a three-ring mesogenic core have been employed in the design of antiferroeletric liquid crystals. Such as Serrano and his

coworkers have synthesized three Schiff base liquid crystals through a carboxylate linkage with terminal (*R*)-2-octyloxy tail exhibited SmC^*, SmA^* phase and antiferroeletric behavior[40]. It can be seen that the mesophase interval of the salicylaldimine-based compound is wider than that of its analogue, the Schiff base molecule on account of the rigidity of the mesogenic nucleus and its polarizability enhanced by intramolecular hydrogen bonding between the hydroxy group and the imine group [41,42]. In addition, the intramolecular hydrogen bonding not only forces molecule to arrange itself in coplanar way but also enhances the intermolecular attraction to make it easy for molecules to array parallel and form a layer structure. This situation was also found at another series of Schiff base compounds, the first ferroelectric SmC^* liquid crystal **DOBAMBC** reported by Meyer[33,43] and its derivative **HDOBAMBC** prepared by Takao.[44]

Recently, we also reported a novel homologous series of chiral salicylaldimine-based liquid crystals in connection with linear alkynyl chain and (*S*)-2-octyloxy tail possessed N^*, $TGBA^*$, SmA^* and SmC_A^* phases.[45] Nevertheless, no chiral Schiff-based liquid crystal with rod-like molecules both possessing frustrated BP and antiferroelectric SmC_A^* phases has been reported until now. In addition, the correlation of chiral Schiff base molecular structure on the appearance of frustrated BP and antiferroelectric (SmC_A^*) phases is still not established. In order

to shed light on the molecular factors on the resulting mesophases in this type of Schiff base compounds, here we report two series of chiral salicylaldimine-based liquid crystals with (*S*)-2-octyloxy tail to investigate the effect of the position of (*S*)-2-octyloxy tail and the length of achiral alkoxy tail on the mesomorphic formation. To best of our knowledge, these simple rod-liked and chiral salicylaldimine-based liquid crystals that possess frustrated blue phase and antiferroelectric behaviors are not reported before. In addition, in order to assess the effect of the intramolecular hydrogen bond on the mesomorphic behavior, corresponding Schiff base compound **H I (n=7)** and **H II (n=8)** without hydroxy group were additionally prepared. We also examine the electro-optic behaviors of the materials under the appropriate applied electric field to prove the antiferroelectric properties of the molecules.

II Results and discussion

II.1 Synthesis and molecular structural characterization

The target chiral Schiff base compounds and their intermediates were synthesized as outlined in Scheme 1. The key amines, 4-alkoxyaniline and 4-[(1*S*)-1-methylheptoxy]aniline were obtained in quantitative yields by catalytic hydrogenation of 4-alkoxynitrobenzene and 4-[1-(1*S*)-methylheptyloxy]nitrobenzene, respectively. The 4-alkoxynitrobenzene

was prepared by known etherification of 4-nitrobenzene with bromoalkane in the presence of K_2CO_3 (process **A**). 4-[1-(1*S*)-methylheptyloxy]nitrobenzene was prepared by Mitsunobu reaction of 4-nitrobenzene with (*R*)-2-octanol (process **B**). The other key intermediates, 4-formyl-3-hydroxyphenyl 4'-[(1*S*)-(1-methylheptyl)oxy]benzoate, 4-formyl-3-hydroxyphenyl 4-(alkyloxy)benzoate and were synthesized by the selective O-alkylation of 2,4-dihydroxybenzaldehye with (*S*)-4-(1-methylheptyloxy)benzoic acid and 4-(alkyloxy)benzoic acid, respectively. 4-Formylphenyl 4'-[(1*S*)-(1-methylheptyl)oxy]benzoate 4-formylphenyl 4-(alkyloxy)benzoate were prepared by the similar method starting from 4-droxybenzaldehye. In the final step, the amines and aldehydes were refluxed in alcohol to perform Schiff base condensation to give the target molecules. The molecular structure of the target dimers and the intermediates were confirmed by spectroscopic analysis and microanalytical data, as described in ESI.†

[Insert Fig. 1 about here]

II.2 Mesophase characterizations and calorimetric studies

The mesophases and transition temperatures and enthalpies for all Schiff base liquid crystals were determined by differential scanning calorimetry (DSC) and polarizing optical microscopy (POM). These results are presented in Table 1 and 2.

Compounds **OH I (n=6, 7)** in which (*S*)-2-octyloxy tail far from the salicylaldimine core exhibits fairly rich polymorphic sequence including frustrated blue phase (BPI) and antiferroelectric SmC_A^* phase that were determined by observation of characteristic textural pattern. For compound **OH I (n= 7)**, on slow cooling (0.2 $°C \cdot min^{-1}$) from their isotropic phase, displays the grazed platelet textural pattern as shown in Fig. 2a, indicating the presence of blue phase (BPI). On further cooling, the paramorphotic defect texture also grow in addition and concomitantly, the characteristic of chiral nematic (N^*) thread-like texture in which dark lines connect two $s = \pm 1/2$ point defects or from closed loops appears as shown in Fig. 2a and full texture shown in ESI.† As the temperature continued to cool down from nematic (N^*) phase, the focal-conic texture appeared, indicating the characteristic of SmA^* phase. On further cooling, the red petal texture start growing and other color petal textures appeared as temperature decline as shown in Fig. 2a. The antiferroelectric SmC_A^* phase appeared as a petal texture and the colors of texture change with temperature caused by the variation of helical pitches with changing temperature in the visible region of the spectrum.[46,47] Compounds **OH I (n=6, 7)** shows a phase transition sequence of Iso.-BPI-N^*-SmA^*-SmC_A^*-Cr. When the achiral alkoxy chain length is extended, the higher homologues **OH I (n=8-12)** shows the absence of frustrated blue phase. This is suggested that an extending the terminal alkoxy chain length

could increase the intermolecular interaction such that diminish the formation of blue phase in this series of Schiff base liquid crystals.

[Insert Table 1. about here]

[Insert Fig. 2 about here]

In order to investigate the correlation of the position of (*S*)-2-octyloxy tail on the formation of frustrated phases, we prepared compounds **OH II (n=6-12)** in which the position of (*S*)-2-octyloxy tail is more closed to the salicylaldimine core. These materials also exhibited more rich polymorphic sequences than compounds **OH II (n=6-12)**. When slow cooling from their isotropic phase, the BPII appeared as iridescent platelet texture as shown in Fig. 2b and Fig. S2 in ESI† for compound **OH II (n=8)** as representative case. Further cooling, The BPI was confirmed by the formation of the grazed plane texture. The colors of both BPII and BPI textures changed with the temperatures were mainly because of the variation of the helical pitches with temperatures. Compound **OH II (n=8)** exhibits chiral nematic (N^*) phase with fan-liked texture, indicating the characteristic of strongly twisted material. On further cooling, the homeotropic (dark) texture of smectic A^* phase and similar a petal texture with compounds **OH I (n=7)**, indicating the characteristic of antiferroelectric SmC_A^* phase as shown in Fig. 2b. Antiferroelectric SmC_A^* phases for compounds **OH I** and **OH II** were further characterized by the Schlieren texture.

It could be seen that two brush and a few of four brush singularities in the Schlieren texture for compound **OH I (n=7)** as shown in Fig. 3a and most of two brush singularities for compound **OH II (n=9)** as shown in Fig. 3b.[36,48,49]

[Insert Table 2. about here]

In addition, in order to study the effect of the intramolecular hydrogen bonding between the hydroxyl group and the imine group on the formation of blue phases and SmC_A^* phases, we also prepared Schiff base compounds **H I (n=7)** and **H II (n=8)** that are in the absence of intramolecular hydrogen bonding and structurally similar with compound **OH I (n=7)** and compound **OH II (n=8)**, respectively. Schiff base compound **H I (n=7)** exhibits similar mesomorphic behavior with compound **OH I (n=7)** except that the blue phase gets eliminated, as shown in Fig. 2c. This SmC_A^* phase was further characterized by the Schlieren texture with most of two-brush singularities, as shown in Fig. 3c. The temperature range of antiferroelectric SmC_A^* phase for compound **I (n=7)** exists from 87.6°C to the crystallization point 59.2°C, is similar with that of compound **OH I (n=7)**. In the other hand, we repeated DSC measurements to examine the stability of Schiff base compound **H I (n=7)**. The DSC thermogrames of the 2nd and 3rd heating-cooling cycles exhibited the similar traces with that of 1st heating-cooling cycles, as shown in ESI.† It can be seen that Schiff base compound **H I (n=7)** is stable under

repeated heating condition. However, Schiff base compound **H II (n=8)** displays BPII, N^* and SmA^* without antiferroelectric SmC_A^* phase. Comparison of mesomorphic behaviors of two Schiff base compounds and their respective structurally similar salicylaldimine-based compounds shows that the mesomorphic interval increases when the rigidity and polarity of mesogenic nucleus are enhanced by intramolecular hydrogen bonding between the hydroxyl group and the imine linkage. Thus salicylaldimine-based compound **OH I (n=7)** displays higher melting point, clearing point and wider mesophase interval (*ca.*10°C) as compared with compound **H I (n=7)**. In addition, wider temperature range of smectic layers can be observed for compound **OH II (n=8)** when compared with compound **H II (n=8)**. These results indicates that the existence of intramolecular hydrogen bonding in the molecular structure possibly enhances the rigidity and the intermolecular attraction of mesogenic nucleus to make it easy for molecules to array parallel and form a layer structure. These tendencies are predictable and similar with mesogenic molecules derived from salicylaldimines, such as previously mentioned ferroelectric SmC^* liquid crystal **HDOBAMBC**[45] as well as antiferroeletric salicylaldimine-based liquid crystals reported by Serrano.[41] These salicylaldimine-based liquid crystals and their each analogues exhibit similar mesomorphic behaviors. In addition, recently, Nandiraju has also reported that

cholesterol-based dimeric Schiff base liquid crystal **KI-4** exhibited frustrated blue phases, N^*, $TGBC^*$ and SmC^* phases.[50] However, the ortho hydroxyl group in the salicylaldimine moiety of the homologue **KI-5(OH)** suppressed the formation of blue phase and widen the temperature range of SmA^* phase. Interestingly, in our case, the presence of intramolecular hydrogen bonding in salicylaldimine-based compounds **OH I (n=6**, **7)** with (*S*)-2-octyloxy tail far from the salicylaldimine core further induces the formation of frustrated fluid structure, BPI. However, when the position of (*S*)-2-octyloxy tail is more closed to the salicylaldimine core, the presence of intramolecular hydrogen bonding in salicylaldimine-based compounds **OH II (n=6-12)** further induces the formation of frustrated fluid structure, antiferroelectric SmC_A^* phase. It means that the two types of the Schiff base molecular structures in conjunction with (*S*)-2-octyloxy tail generates high chirality. The plot of temperature vs the length achiral alkoxy tail (*n*) (Fig. 4) shows the increasing *n* decreases melting point and depresses the formation of frustrated fluid blue phase for compounds **OH I** with (*S*)-2-octyloxy tail far from the salicylaldimine core. However, Fig. 5 shows the increasing *n* destabilize the formation of antiferroelectric SmC_A^* phase for compounds **OH II** with (*S*)-2-octyloxyl tail close to the salicylaldimine core. Notably, compound **OH II(n=7)** exhibits the most wide temperature range of antiferroelectric SmC_A^* phase (45°C) and compound **OH**

II(n=12) displays the lack of antiferroelectric SmC_A^* phase. Therefore, it can be seen that the increasing of the achiral alkoxy tail (*n*) supports the formation of layered structure to widen the interval of smectic mesophases, especially SmA phase that molecules are parallel to the layer normal.

[Insert Fig. 4 about here]

[Insert Fig. 5 about here]

II. 3 Electrical switching study.

The antiferroelectric SmC_A^* phase also further characterized from the switching current and dielectric permittivity measurements. The triangular wave is the most effective among DC, square and triangular waveforms for the alignment recovery of antiferroelectric liquid crystal molecules.[51] In addition, the appearance of two switching current peaks means the instance of the transmittance changes, indicating the switchings from and to the third stable state occur at different voltages.[28] We take compound **OH II (n=7)** as representative materials for these measurements. The switching current behaviors of them were measured in 5 μm homogeneously aligned cell, and the switching profiles are presented in Fig. 6. For compound **OH II (n=7)**, besides a broad current peak was found close to zero field point due to the ionic effect, it is seen that there are two switching current peaks appeared simultaneously located approximately at opposite side of zero field point on an

applying triangular wave and, representing the antiferroelectric-ferroelectric and ferroelectric-ferroelectric switchings in the SmC_A^* phase, similar to that reported previously in **MHPOBC**.[30]

[Insert Fig. 6 about here]

In clarifying the characteristic and determining the origin of the layer switching, microscope observation of the texture upon application of the triangular wave field serves as a useful method. Fig. 7 shows texture change of compounds **OH I(n=7)** by turning on and off an electric field in SmC_A^* phase. Before the application of an electric field, ellipse-hyperbola focal conics are observed in 5μm homogeneously aligned cell. With the application of the triangular wave field (50Hz, $5V_{pp}$), the texture changes in such a way that ellipse-hyperbola focal conics gradually disappeared. When the field is turn off, microscopic striped pattern of the homogeneous texture appeared. This possibly suggests that dechiralization lines are perpendicular to the layer normal and the ferroelectric domains appeared. This first change of defects is irreversible. However, the texture changes reversibly between Fig. 7b and Fig. 7c during the subsequent switching.[52] In addition, Fig. 8 and Fig. 9 also show the electric-field-induced textural changes of compound **H II(n=7)** and compound **OH II(n=7)**, respectively, indicating the similar switching behaviors with compound **OH I(n=7)**.

[Insert Fig. 7 about here]

[Insert Fig. 8 about here]

[Insert Fig. 9 about here]

The temperature dependence of the dielectric constants ε' measured at 100 Hz in the 25 μm homogeneously aligned cell was investigated. The represented results for compound **OH II(n=7)** from the cooling measurements are shown in Fig. 10. During cooling, the dielectric constants ε' in the SmA^* phase are small and slightly increase at the SmA^* to SmC_A^* transition. The characteristic points corresponding to the SmA^* to SmC_A^* transition is seen as a small peak at approximately from 85°C to 87°C. Since the macroscopic polarization from ferroelectric contribution does not exist in the antiferroelectric phase, the contribution of the Goldstone mode (the small winding and unwinding motions of helical structure) cannot be detected by the means of the dielectric measurement, thus, the enhancement of the dielectric constant in the antiferroelectric phase is considered to be the result of the antiferroelectric soft mode[53] and the vibration of the azimuthal molecular motion.[54] Moreover, a broad peak shown in the antiferroelectric phase possibly resulted from the weaker vibration of the azimuthal molecular motion. Similar trends for other compounds such as **OH I(n=7)** and **H I(n=7)** could also be observed, as shown in ESI.† There has no existence of Goldstone relaxation in the SmC_A^* phase, further

demonstrating the existence of antiferroelectric property. All of the results from switching behaviors and dielectric permittivities are similar to our previous reported antiferroelectric salicylaldimine-based compounds **$C_mYCBOC_8^*$(m=6-10)** having (*S*)-2-octyloxy tail.

[Insert Fig. 10 about here]

III. Conclusion

In this article, we have described the synthesis and thermotropic properties of two series of chiral salicylaldimine-based liquid crystals having (*S*)-2-octyloxy tail with two different positions. Two homologues have been investigated with the correlation of the position of (*S*)-2-octyloxy tail on the frustrated blue phase and antiferroelectric (SmC_A^*) phase. In addition, the length of achiral alkoxy tail has been varied from hexyloxy to dodecyloxy tail with the intention of understanding the structure and property relationship. In general, the majority of chiral salicylaldimine-based liquid crystals exhibit antiferroelectric (SmC_A^*) phase. For compound **OH I(n=6-12)** in which (*S*)-2-octyloxy tail far from the salicylaldimine core, frustrated blue phase destabilize and the temperature range of SmC_A^* phase extends as the length of the achiral alkoxy tail (*n*) increases. For compound **OH II(n=6-12)** with (*S*)-2-octyloxy tail close to the salicylaldimine core, all of compounds exhibit BPII and BPI. However, the length increasing of the achiral

alkoxy tail depresses the stability of antiferroelectric SmC_A^* phase. Only chiral salicylaldimine-based compound **OH II(n=12)** exhibits the lack of antiferroelectric SmC_A^* phase. In addition, Schiff base compounds **H I(n=7)** without hydroxy group also exhibits antiferroelectric SmC_A^* phase but no blue phase sequence. However, Schiff base compounds **H II(n=8)** without hydroxy group exhibits BPII phase but no antiferroelectric property. It can be seen that the existence of the intramolecular hydrogen bonding in the chiral salicylaldimine-based compounds **OH I** with achiral alkoxy tail close to the salicylaldimine core could enhance the rigidity and polarity of mesogenic nucleus and further induce the formation of frustrated blue phase. However, the antiferroelectric property of the chiral salicylaldimine-based compounds **OH II** with (*S*)-2-octyloxy tail close to the salicylaldimine core could result from the intermolecular attraction of mesogenic nucleus to array parallel and form a layer structure. It can be concluded that this type of Schiff base compounds in conjunction with (*S*)-2-octyloxy tail generate high chirality to easily exhibit BP and antiferroelectric SmC_A^* phase. More related compounds will be studied and reported on the correlation of molecular structure to the appearance of blue phase and SmC_A^* phase in the nearest future.

Acknowledgements

We thank the financial support from the National Science Council of Taiwan (*R.O.C.*) through NSC99-2113-M-036-001-MY2 and Tatung University through B103-C04-008.

References

1. D. Demus, J. Goodby, G. W. Gray, H.-W. Spiess and V. Vill, *Handbook of Liquid Crystals*, Wiley-VCH, New York, USA. 1998.
2. P. Crooker, in *Chirality in Liquid Crystals*, ed. H.-S. Kitzerow and C. Bahr, Springer, New York, 2001.
3. H. Kikuchi, *Struct. Bonding*, 2008, **128**, 99-117.
4. H.-S. Kitzerow, *ChemPhysChem*, 2006, **7**, 63-66.
5. C. V. Yelamaggad, I. S. Shashikala, G. Liao, D. S. Shankar Rao, S. K. Prasad, Q. Li, and A. Jákli, *Chem. Mater.*, 2006, **18**, 6100–6102.
6. A. Yoshizawa, M. Sato and J. Rokunohe, *J. Mater. Chem.*, 2005, **15**, 3285-3290.
7. M. Sato and A. Yoshizawa, *Adv. Mater.*, 2007, **19**, 4145-4148.
8. H. Iwamochi, T. Hirose, Y. Kogawa and A. Yoshizawa, *Chem. Lett.*, 2010, **39**, 170-171.
9. H. Kikuchi, M. Yokota, Y. Hisakado, H. Yang and T. Kajiyama, *Nat. Mater.*, 2002, **1**, 64–68.
10. E. Karatairi, B. Rozic, Z. Kutnjak, V. Tzitzios, G. Nounesis, G. Cordoyiannis, J. Thoen, C. Glorieux and S. Kralj, *Phys. Rev. E: Stat., Nonlinear, Soft Matter Phys.*, 2010, **81**, 041703/1-041703/5.
11. W. He, G. Pan, Z. Yang, D. Zhao, G. Niu, W. Huang, X. Yuan, J. Guo, H. Cao and H. Yang, *Adv. Mater.*, 2009, **21**, 2050–2053.
12. H. J. Coles and M. N. Pivnenko, *Nature*, 2005, **436**, 997-1000.
13. M. Lee, S. T. Hur, H. Higuchi, K. Song, S. W. Choi and H. Kikuchi, *J. Mater. Chem.*, 2010, **20**, 5813-5816.
14. Z. Zheng, D. Shen and P. Huang, *New J. Phys.*, 2010, **12**, 113018/1-113018/10.
15. S. Taushanoff, K. V. Le, J. Williams, R. J. Twieg, B. K. Sadashiva, H. Takezoe and A. Jákli, *J. Mater. Chem.*, 2010, **20**, 5893-5898.

16. Y. Kogawa and A. Yoshizawa, *Liq. Cryst.* 2011, **38**, 303-307.
17. K.V. Le, S. Aya, Y. Sasaki, H. Choi, F. Araoka, K. Ema, J. Mieczkowski, A. Jákli, K. Ishikawa and H. Takezoe, *J. Mater. Chem.,* 2011, **21**, 2855–2857.
18. L. Wang, L. Yu, X. Xiao, Z. Wang, W. He, P. Yang and H. Yang, *Liq. Cryst.,* 2012, **39**, 629-638.
19. A. Yoshizawa, *J. Soc. Inf. Disp.,* 2008, **16**, 1189−1194.
20. H. Iwamochi and A. Yoshizawa, *Mol. Cryst. Liq. Cryst.,* 2009, **509**, 223−232.
21. M. Nakata, Y. Takanishi, J. Watanabe and H. Takezoe, *Phys. Rev. E,* 2003, **68**, 41710-41716.
22. H. Iwamochi, T. Hirose, Y. Kogawa and A. Yoshizawa, *Chem. Lett.,* 2010, **39**, 170−171.
23. H. Iwamochi, T. Hirose, Y. Kogawa and A. Yoshizawa, *Chem. Lett.,* 2010, **39**, 170−171.
24. Park, K.-W.; Gim, M.-J.; Kim, S.; Hur, S.-T.; Choi, S.-W. *ACS Appl. Mater. Interfaces,* 2013, **5**, 8025−8029.
25. I-H. Chiang, C.-J. Long, H.-C. Lin, W.-T. Chuang, J.-J. Lee and H.-C. Lin, *ACS Appl. Mater. Interfaces,* 2014, **6**, 228-235.
26. H. Grebel, R. M. Hornreich and S. Shtrikman, *Phys. Rev. A,* 1983, **28**, 1114−1138.
27. V. A. Belyakov, E. I. Demikhov, V. E. Dmitrienko and V. K. Dolganov, *J. Exp. Theor. Phys.* 1985, **62**, 1173−1182.
28. A. D. L. Chandani, T. Hagiwara, Y. Suzuki, Y. Ouchi, H. Takezoe and A. Fukuda, *Jpn. J. Appl. Phys.,* 1988, **27**, L729-L732.
29. A. D. L. Chandani, Y. Ouchi, H. Takezoe, A. Fukuda, K. Terahima, K. Furukawa and A. Kishi, *Jpn. J. Appl. Phys.,* 1989, **28**, L1261-L1264.
30. A. Fukuda, Y. Takanishi, T. Iasozki, K. Ishikawa, H. Takezoe, *J. Mater. Chem.,* 1994, **4**, 997-1016.
31. J. W. Goodby, A. J. Slany, C. J. Booth, I. Nishyama, J. D. Vuijk, P. Syring and K. J. Toyne, *Mol. Cryst. Liq. Cryst.,* 1994, **243**, 231-298.
32. S. T. Lagerwall, *Ferroelectric and Antiferroelectric Liquid Crystals*, Wiley-VCH, Weinheim, New York, 1999.
33. M. Hird, *Liq. Cryst.*, 2011, **38**, 1467–1493.
34. M.-H. Li, L. Detre, P. Cluzeau, N. Isaert and H.-T. Nguyen, *Liq. Cryst.,* 1998, **24**, 347-359.
35. J. P. F. Lagerwall, F. Giesselmann, M. D. Wand and D. M. Walba, *Chem. Mater.,* 2004, **16**, 3606–3615.
36. S.-L.Wu and W.-J. Hsieh, *Chem. Mater.*, 1999, **11**, 852-854.
37. S.-L. Wu and W.-J. Hsieh, *Chem. Mater.*, 2003, **15**, 4515-4520.

38. J. L. Serrano and T. Sierra, *Metallomesogens, ed.*, Wiley-VCH, Weinheim, 1996.
39. T. Seshadri and H. Haupt, *Chem. Comm.,* 1998, 735-736.
40. D. L. de Murillas, R. Piñol, M. B. Ros, J. L. Serrano, T. Sierra and M. R. de la Fuente, *J. Mater. Chem.,* 2004, **4**, 1117-1127.
41. T. Tian, X. Xu, Y Zhao and X. Tang. *Liq Cryst.*, 1995, *19*, 295-300
42. T. Sierra, E. Meléndez, J. L. Serrano, A. Ezcurra and M. A. Pérez-Jubindo, *Chem. Mater.*, 1991, **3**, 157-163.
43. R. B. Meyer, L. Liebert, L. Strzelecki and P. Keller, *J. Phys. Lett. (Paris).,* 1975, **36**, L69-L71.
44. S. Takao, S. Kazutami, H. Masao, Y. Katsumi and O. Masanori, *Ferroelectrics,* 1984, **58**, 21-32.
45. C. C. Huang, C. C. Kao, N. C. Wang, M. C. Yu and S. L. Wu, *Liq. Cryst.,* 2013, **40**, 441-445.
46. S. Inui, N. Iimura, T. Suzuki, H. Iwane, K. Miyachi, Y. Takanishi and A. Fukuda, *J. Mater. Chem.,* 1996, **6**, 671-673.
47. I. Nishyama, E. Chin and J. W. Goodby, *J. Mater. Chem.,* 1993, **3**, 161-168.
48. P. Gisse, J. Pavel, H. T. Nguyen and V. L. Lorman, *Ferroelectrics*, 1993, 147, 27-41.
49. S. L. Wu and C. T. Chiang, *Liq. Cryst.,* 2002, **29**, 39-45.
50. D. D. Sarkar, R. Deb, N. Chakraborty, G. Mohiuddin, R. K. Nath and V.S. Rao Nandiraju, *Liq. Cryst.,* 2013, **40**, 468-481.
51. K. Itoh, M. Johno, Y. Takanishi, Y. Ouchi, H. Takezoe and A. Fukuda, *Jpn. of Appl. Phys.,* 1991, **30**, 735-740.
52. Y. I. Suzuki, T. Isozaki, S. Hashimoto, T. Kusumoto, T. Hiyama, Takanishi, T. H. Takezoe, and A. Fukuda, *J. Mater. Chem.,* 1996, **6**, 753-760.
53. S. Hiller, S. A. Pikin, W. Haase, J. W. Goodby and I. Nishiyama, *Jpn. J. of Appl. Phys.,* 1994, **33**, L1170-L1173.
54. M. Buivyads, F. Gouda, G. Andersson, S. T. Lagerwall, B. Stebler, J. Bomelburg, G. Heppke and B. Gestblom, *Liq. Cryst.,* 1997, **23**, 723-729.

Graphical Abstract

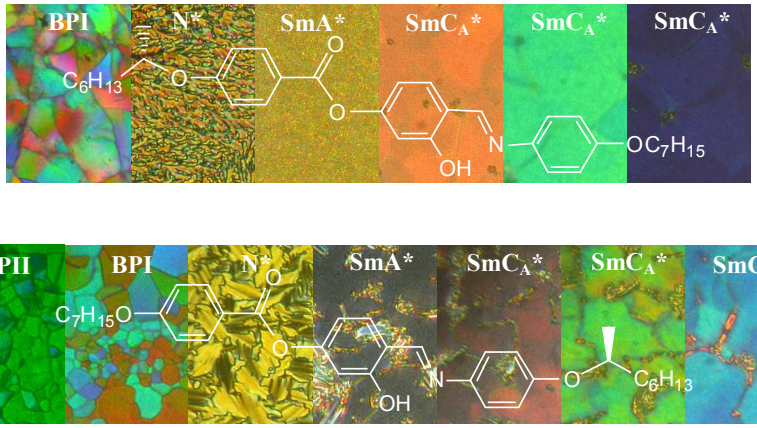

Chiral salicylaldimine-based liquid crystals in which (*S*)-2-octyloxyl tail close to or far from the salicylaldimine core possess frustrated blue phase and antiferroelectric SmC_A^* phase.

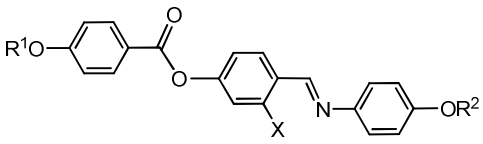

Compounds	X	R^1	R^2
OH I (n = 6-12)	OH	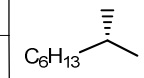	
H I (n = 7)	H		
OH II (n = 6-12)	OH	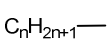	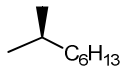
H II (n = 8)	H		

Fig. 1 Chemical structures of compound **OH I (n=6-12)**, **OH II (n=6-12)**, **H I (n=7)** and **H I (n=8)**

(a)

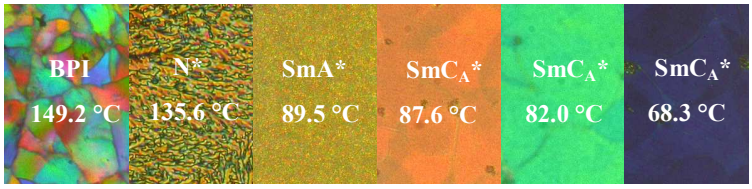

(b)

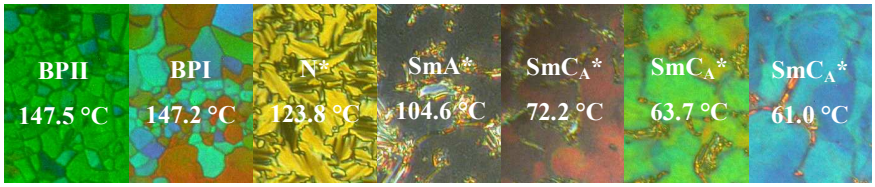

(c)

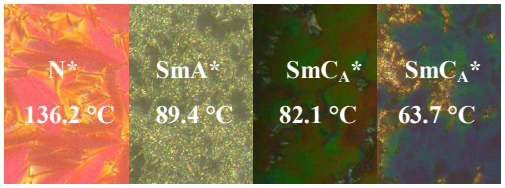

(d)

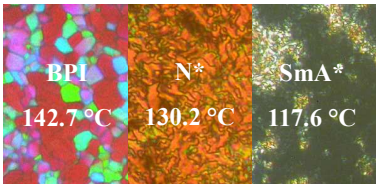

Fig. 2 Microphotographic textures of the mesomorphic phases obtained from (a): **OH I (n=7)** (b): **OH II (n=8)** (c): **H I (n=7)** (d): **H II (n=8)** at various mesogenic phase temperatures (magnification × 400).

(a) (b)

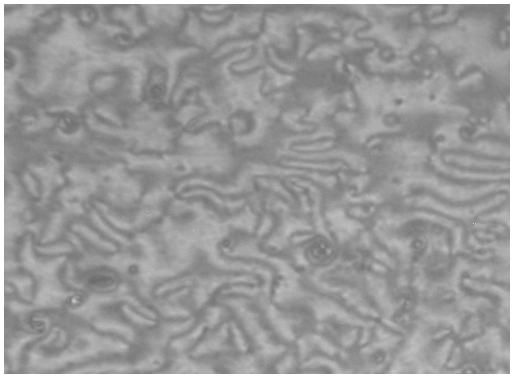

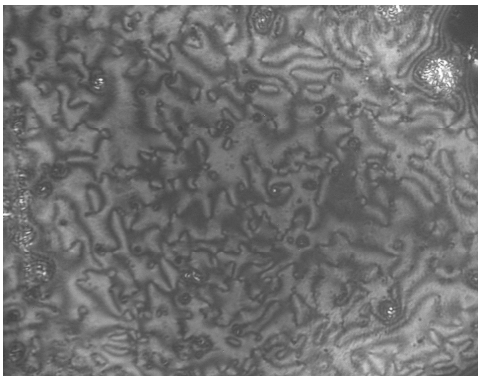

(c)

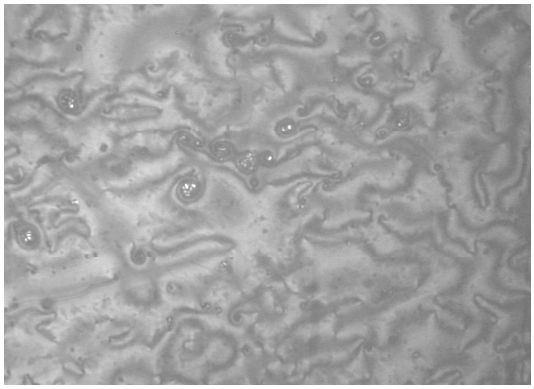

Fig. 3 Microphotomorphic textures: (a) Schlieren texture displaying both two- and four-brush singularities of the SmC_A^* phase obtained from compound **OH I (n=7)** at 82.2 °C. (b) Schlieren texture displaying most of two-brush singularities of the SmC_A* phase obtained from compound **H I (n=7)** at 66.4 °C. (c) Schlieren texture displaying most of two-brush singularities of the SmC_A* phase obtained from compound **OH II (n=9)** at 60.5 °C (magnification × 400).

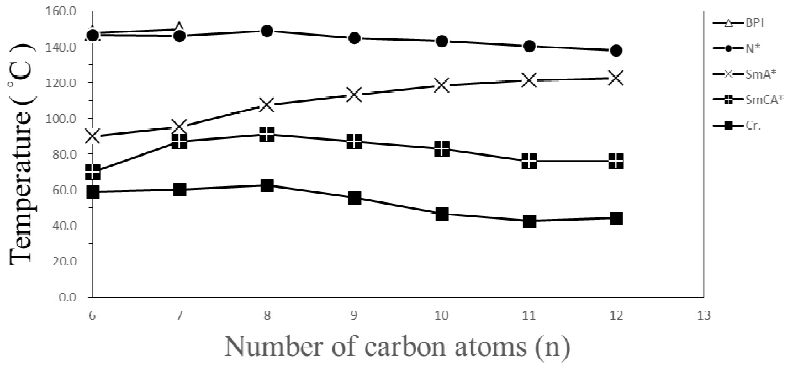

Fig. 4 Plot of transition temperatures as achiral alkoxy tail length (*n*) for compounds **OH I (n)**.

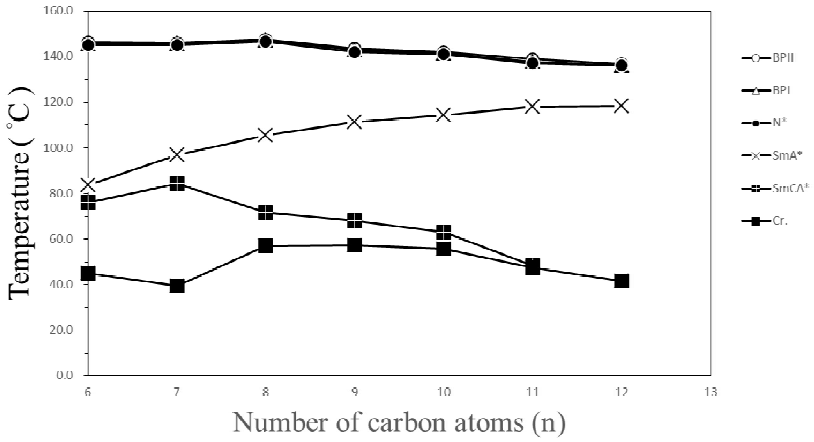

Fig. 5 Plot of transition temperatures as achiral alkoxy tail length (*n*) for compounds **OH II (n)**.

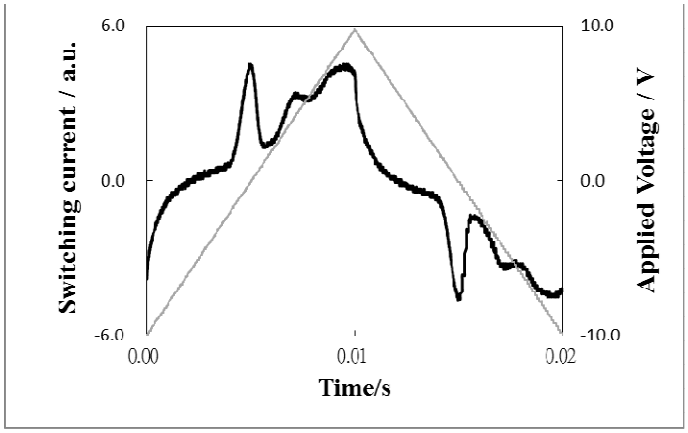

Fig. 6 Switching current in a triangle electric field (50 Hz, 6 V_{pp}) in the SmC_A^* phase at 82.0 °C for compound **OH II (n=7)** in 5 μm thickness of homogeneously aligned cell.

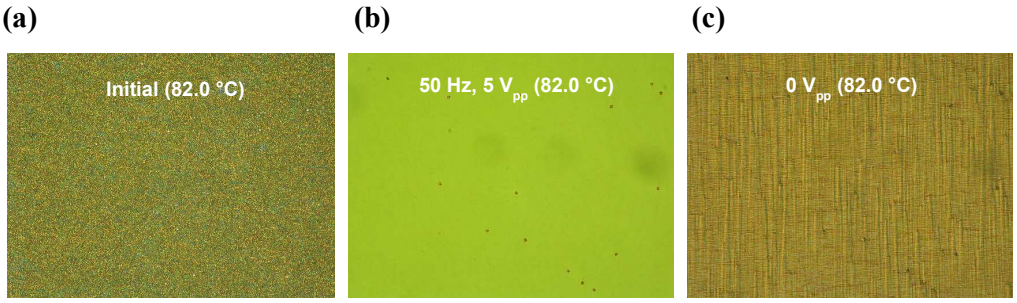

Fig. 7 Electric-field-induced textural changes observed at 82.0°C in a 5.0 µm thickness of homogeneously aligned cell of compound **OH I (n=7)**

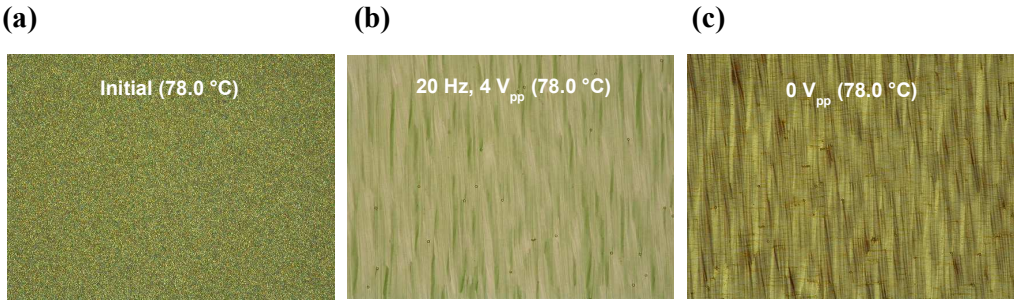

Fig. 8 Electric-field-induced textural changes observed at 78.0°C in a 5.0 µm thickness of homogeneously aligned cell of compound **H I (n=7)**

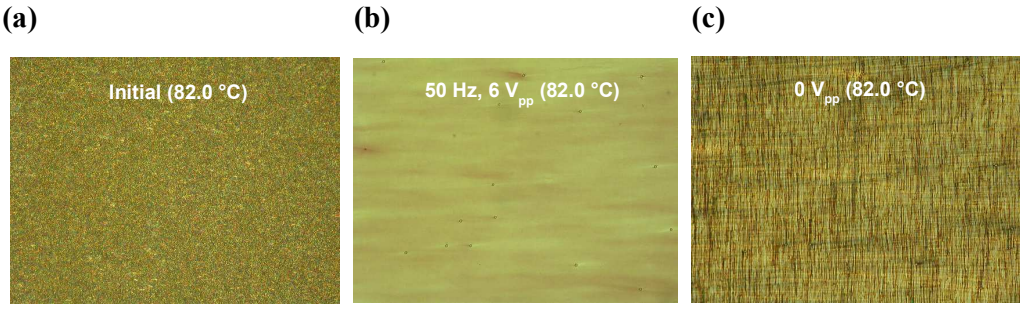

Fig. 9 Electric-field-induced textural changes observed at 82.0°C in a 5.0 µm thickness of homogeneously aligned cell of compound **OH II (n=7)**

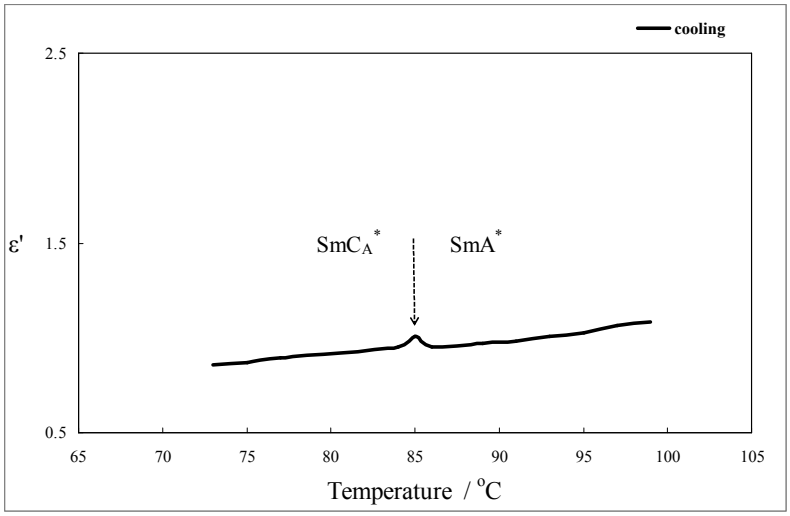

Fig. 10 Temperature dependence of the dielectric constant ε′ for compound **OH II (n=7)** at 100 Hz in the cell with 25 μm thickness under 1°C min^{-1} cooling process.

Table 1. Mesophases, transition temperatures (°C) and enthalpies ΔH (in brackets, kJ·mol^{-1}) of compounds **OH I (n=6-12)** recorded from DSC thermograms at heating/cooling rate of 3°C·min^{-1}.

Compound	Iso		BPI		N*		SmA*		SmC_A*		Cr.[a]	mp.[b]
OH I (n=6)	•	147.7 [1.1]	•	146.6[c] d	•	90.1 [0.6]	•	70.0[c] e	•	58.8 [19.6]	•	89.9 [22.6]
OH I (n=7)	•	149.6 [1.6]	•	146.0[c] d	•	95.1 [0.6]	•	87.0[c] e	•	60.0 [28.9]	•	87.2 [26.5]
OH I (n=8)	•	149.0[c] [0.75]	—		•	107.6 [0.8]	•	91.0 e	•	62.5 [19.6]	•	92.2 [22.6]
OH I (n=9)	•	144.7[c] [0.7]	—		•	113.2 [1.0]	•	87.0[c] e	•	55.6 [11.4]	•	88.4 [19.7]
OH I (n=10)	•	143.4[c] [1.0]	—		•	118.6 [1.3]	•	83.0[c] e	•	46.7 [20.3]	•	80.0 [25.5]
OH I (n=11)	•	140.4[c] [0.8]	—		•	121.3 [1.5]	•	76.0[c] e	•	42.7 [18.4]	•	67.9 [21.8]
OH I (n=12)	•	138.1[c] [1.1]	—		•	122.6 [1.7]	•	76.0[c] e	•	44.2 [19.8]	•	67.2 [23.4]

[a]Cr. refers to crystal. [b]m.p. refers to melting point taken from DSC thermograms recorded at heating rates of 3°C·min^{-1}. [c]The phase transition temperature was determined by optical microscopy at cooling rate of 0.1°C·min^{-1}. [d]The enthalpy of BPI-N* transition wad added into that of Iso-BPI transition. [e]The enthalpy of phase transition was too small to be determined at cooling rate of 3°C·min^{-1}

Table 2. Mesophases, transition temperatures (°C) and enthalpies ΔH (in brackets, $kJmol^{-1}$) of compounds **OH II (n=6-12)** recorded from DSC thermograms at heating/cooling rate of $3°C·min^{-1}$.

Compound	Iso	BPII	BPI	N*	SmA*	SmC_A*	Cr.[a]	mp.[b]
OH II (n=6)	• 146.4 [0.9]	• 145.6[c] d	• 145.2 d	• 83.7 [1.2]	• 76.0[c] e	• 45.1 [19.1]	•	93.1 [28.2]
OH II (n=7)	• 146.1 [1.0]	• 145.7[c] d	• 145.2 d	• 97.0 [1.9]	• 84.3[c] e	• 39.3 [18.7]	•	80.7 [27.2]
OH II (n=8)	• 147.6 [0.9]	• 147.2[c] d	• 146.6 d	• 105.6 [1.9]	• 71.6[c] e	• 56.8 [22.1]	•	80.8 [23.7]
OH II (n=9)	• 143.5 [0.9]	• 143.0[c] d	• 142.2 d	• 111.4 [1.9]	• 68.1[c] e	• 57.1 [23.3]	•	86.0 [29.3]
OH II (n=10)	• 142.0 [0.9]	• 141.4[c] d	• 141.1 d	• 114.4 [2.1]	• 63.1[c] e	• 55.6 [23.1]	•	90.0 [28.2]
OH II (n=11)	• 139.0 [1.3]	• 137.7[c] d	• 137.1 d	• 118.1 [3.2]	• 48.3[c] e	• 47.4 [24.7]	•	79.3 [32.2]
OH II (n=12)	• 136.9 [1.6]	• 136.3[c] d	• 136.1 d	• 118.5 [2.8]	•	— 41.5 [23.2]	•	65.6 [26.5]

[a]Cr. refers to crystal. [b]m.p. refers to melting point taken from DSC thermograms recorded at heating rates of $3°C·min^{-1}$. [c]The phase transition temperature was determined by optical microscopy at cooling rate of $0.1°C·min^{-1}$. [d]The enthalpy of BP-N* transition wad added into that of Iso-BPII transition. [e]The enthalpy of phase transition was too small to be determined at cooling rate of $3°C·min^{-1}$

Table 3. Mesophases, transition temperatures (°C) and enthalpies ΔH (in brackets, kJmol^{-1}) of compounds **I** and **II** recorded from DSC thermograms at heating/cooling rate of 3°C·min^{-1}.

Compound	Iso		BPII		N*		SmA*		SmC_A*		Cr.[a]		mp.[b]
I (n=7)	•	138.9 [1.8]	—		•	90.7 [2.1]	•	87.6[c] e	•	59.2 [33.1]	•		77.0 [26.9]
II (n=8)	•	144.4 [1.1]	•	143.8[c] d	•	121.0 [0.6]	•		—	65.1 [38.3]	•		86.6 [37.6]

[a]Cr. refers to crystal. [b]m.p. refers to melting point taken from DSC thermograms recorded at heating rates of 3°C·min^{-1}. [c]The phase transition temperature was determined by optical microscopy at cooling rate of 1°C·min^{-1}. [d]The enthalpy of BPII-N* transition wad added into that of Iso-BPII transition. [e]The enthalpy of phase transition was too small to be determined at cooling rate of 3°C·min^{-1}